Int. J. Heat Mass Transfer. Vol. 12, pp. 1109–1121. Pergamon Press 1969. Printed in Great Britain

MEASUREMENTS OF AVERAGE HEAT TRANSFER COEFFICIENTS FOR A MESH SIMULATING POROUS PARACHUTE CLOTH

C. J. SCOTT†, E. R. G. ECKERT‡ and M. RUIZ-URBIETA§

Heat Transfer Laboratory, Department of Mechanical Engineering, University of Minnesota, Minneapolis, Minnesota 55455

(*Received* 29 *July* 1968 *and in revised form* 30 *January* 1969)

Abstract—Experimental heat transfer studies have been performed on three screens simulating a porous parachute. The average Nusselt number was measured as a function of the sonic Reynolds number. The range of the sonic Reynolds number extended from 5 to about 1400. Three different porosities and two different pressure ratios were used.

The relation

$$\frac{Nu^*}{(Re^*)^{\frac{1}{2}}}\ \frac{L+D}{L} = 0{\cdot}5$$

appears to be an acceptable representation of the average Nusselt number on the screen for sonic Reynolds number above 400. Below this sonic Reynolds number rarefaction effects influence the average Nusselt number. No effect of the porosity could be detected; while the influence of the ratio of the upstream pressure to the downstream static pressure was small for the two values tested.

NOMENCLATURE

A, convective heat-transfer area [ft^2];
a, speed of sound [ft/s];
d, wire diameter [ft];
h, average convective heat transfer coefficient [Btu/hft^2°F];
I, intensity of electrical current [amp];
k, thermal conductivity (Btu/hft°F);
Kn, Knudsen number;
L, distance between wire edges;
Ma, Mach number;
Nu, Nusselt number, $= hd/k_0$;
P_{up}, absolute total pressure upstream of the nozzle [mm of Hg];
P_{down}, absolute static pressure downstream of test mesh [mm of Hg];
Po, geometric porosity;
q, heat flux [Btu/hft^2];
R, electrical resistance of test mesh [ohm];
Re, sonic Reynolds number, $= \rho^* a^* d/\mu^*$;
T, t, temperature [°R, °F];
u, velocity [ft/s];
α, temperature resistance coefficient [°F^{-1}];
ρ, density [lb$_m$/ft^3];
μ, viscosity [lb$_m$s/ft^2].

Superscripts

* sonic conditions, assuming isentropic expansion to sonic velocity.

Subscripts

aw, adiabatic wall conditions;
f, flight conditions;
0, reference value;
w, conditions of the screen's wires;
up, 1, conditions upstream of the grid;
$down$, conditions downstream of the grid.

† Associate Professor.
‡ Regents' Professor and Director, Thermodynamics and Heat Transfer.
§ Research Assistant

1. INTRODUCTION

IT IS well known that by the aerodynamic heating effect, vehicles which fly at supersonic speeds, are heated to such an extent that the skin temperatures and the temperatures inside the craft require the special attention of the designer. In addition, a growing interest in aircraft vehicle recovery operations has directed attention to a variety of deceleration devices. In many cases a sizeable portion of the initial kinetic energy of the vehicle is converted into an increase in internal energy of the retardation device and the aerodynamic heat transfer of the deceleration device becomes a design factor.

Aerodynamic decelerators must possess a large drag-to-weight ratio and normally must be capable of being stored in a small volume. Therefore, most drag-producing devices are relatively thin and flexible. Towed decelerators such as ribbon or hyperflo parachutes, balloons, ballutes, etc., have flexible canopies. Other proposals incorporate structural members (cones or paragliders) or hybrid systems such as AVCO drag brake [1] and the NASA rotornet [2].

Most impermeable retardation devices are aerodynamically unstable when utilized in a supersonic flow. As a result, nearly all of the retardation devices discussed above employ extended porous surfaces in conjunction with venting techniques (see Fig. 1). Most conventional textile fibers either melt or are seriously degraded by exposure to temperatures above 500°F. It is desirable to replace these fibers with materials of higher thermal durability such as fine metallic wires in which operational temperatures are close to 2000°F.

The flow field associated with a parachute results from the interaction of the large-scale phenomena enveloping the complete body and the small-scale processes associated with the local flow through a single porous element in the mesh material itself. The large-scale phenomena (parachute shape and size, velocity, altitude), which vary with the particular design, are generally involved with the aerodynamics of the problem and contribute end or boundary conditions (pressure ratio, Reynolds number) to the small-scale phenomena.

When opened at a flight Mach number exceeding unity, a parachute produces a bow shock immediately forward of the canopy. The flow impinging on the parachute fabric is subsonic and normal to the surface except near the periphery of the canopy [3]. Hence, for most of the surface area of the parachute an appropriate model is a woven mesh with the flow impinging normal to it. The flow is isentropically expanded to sonic conditions at the minimum area of the mesh, based on the open porosity of the canopy roof, and then further expands into supersonic jets bordered by free shear layers downstream (small-scale

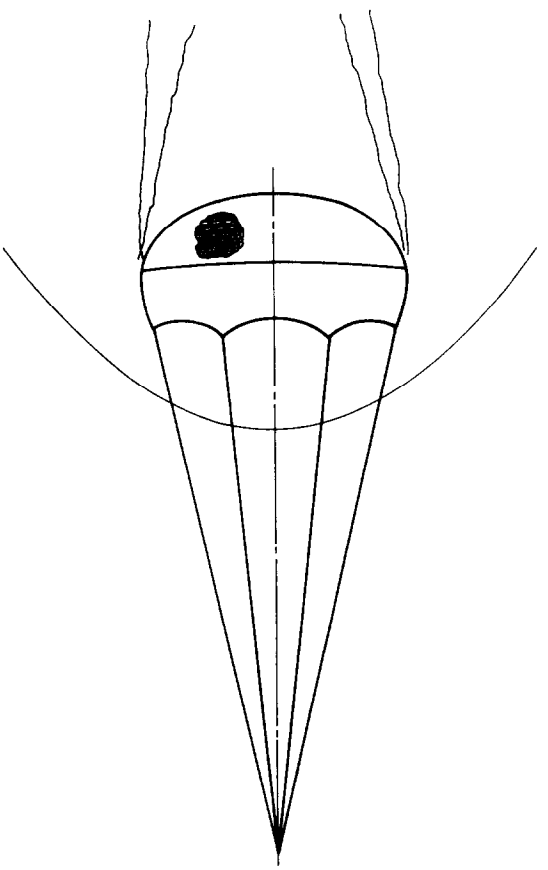

FIG. 1. Sketch of a porous parachute.

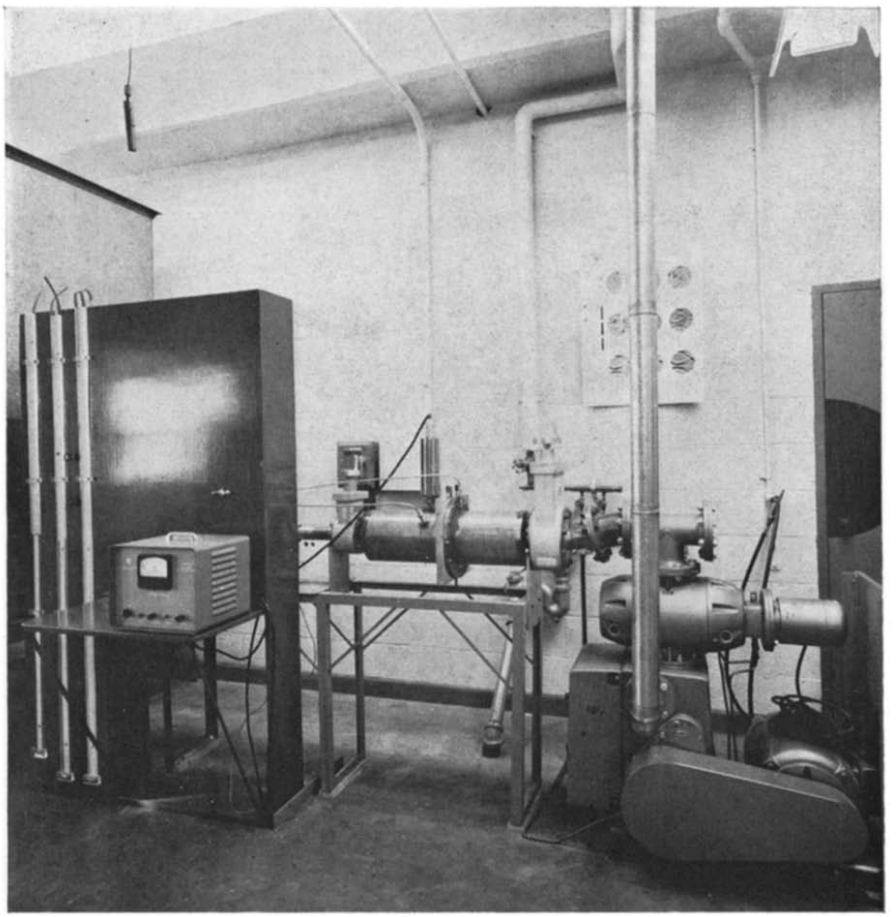

FIG. 2. Photograph of the wind tunnel.

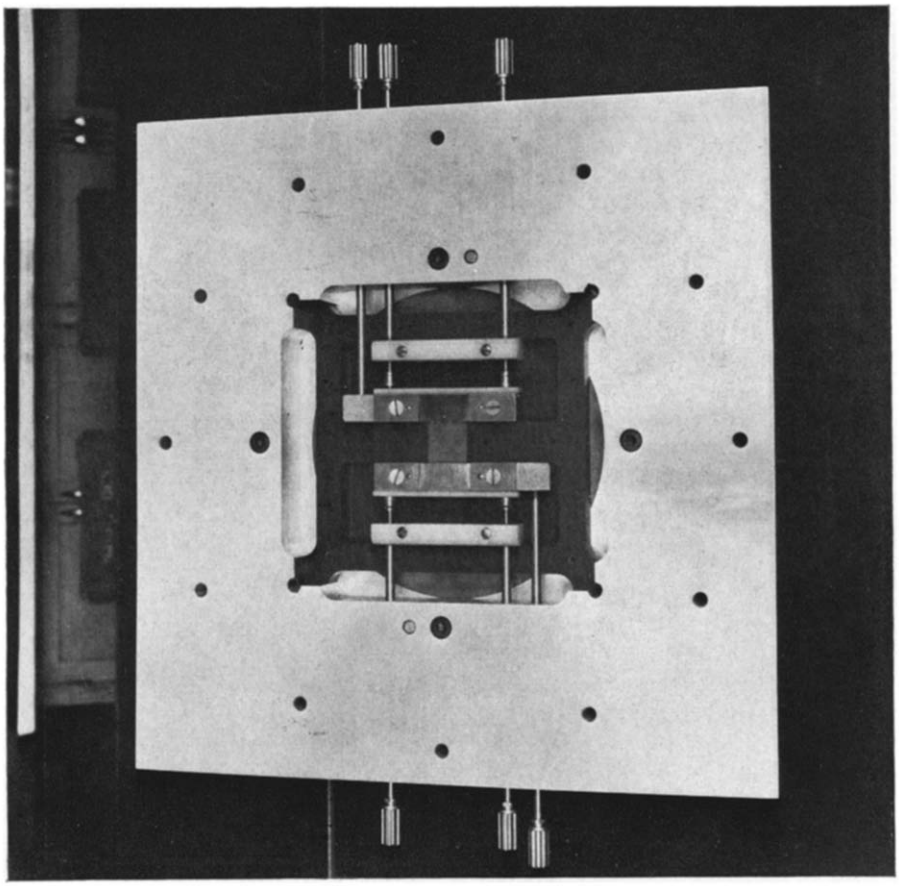

FIG. 5. Aluminum plate with test section and housing blocks.

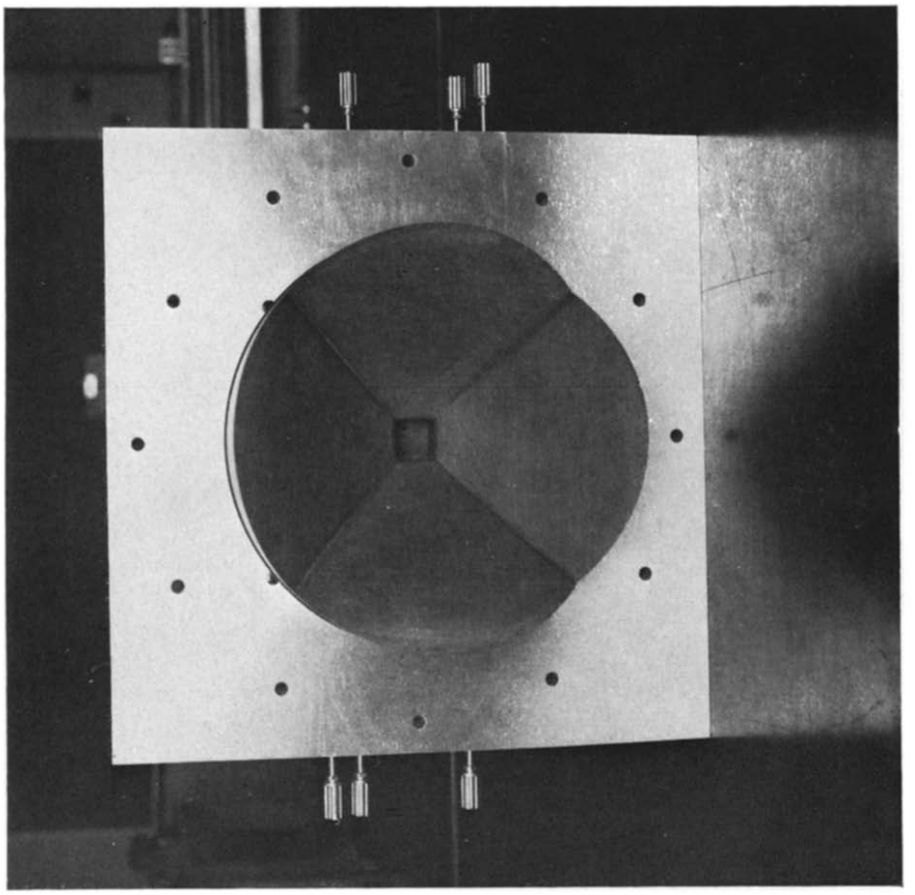

FIG. 6. Aluminum plate with nozzle.

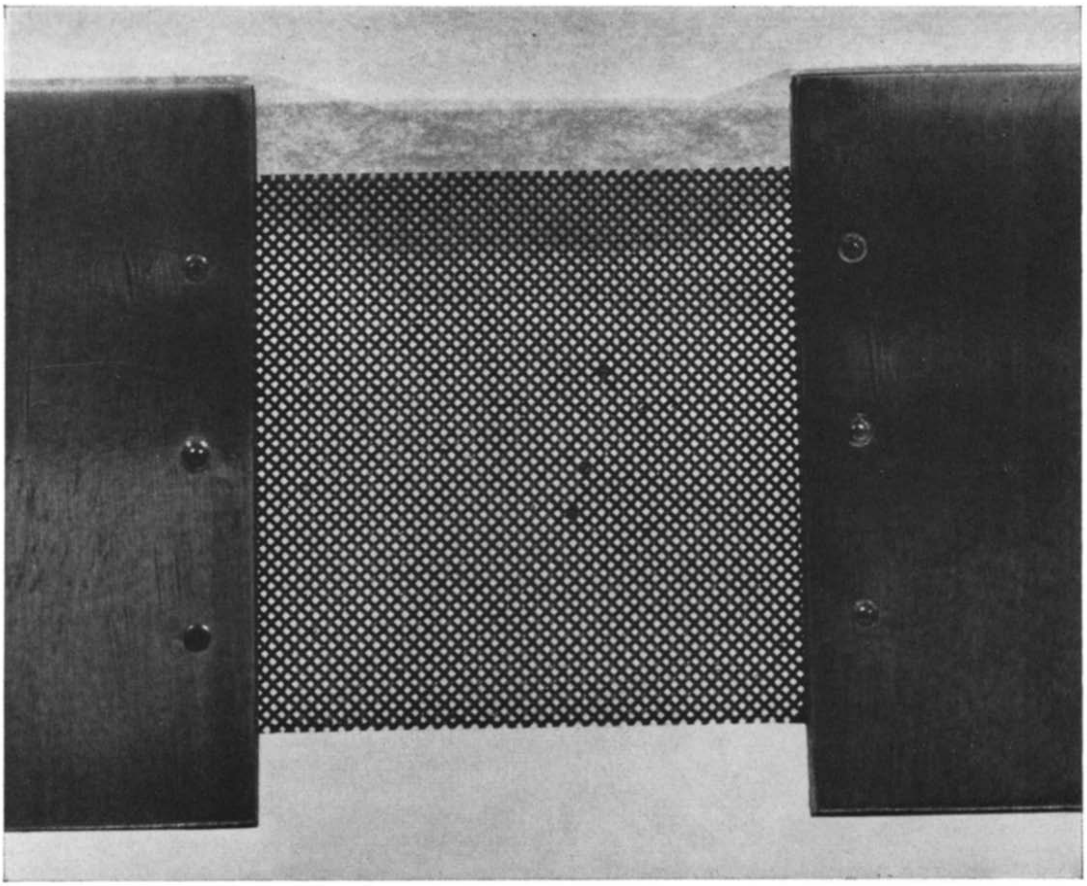

FIG. 7. One test screen.

phenomena). Immediately behind each individual fiber a small region of recirculating, subsonic vortex-flow exists.

Most parachutes are constructed of fabrics which are very poor thermal conductors. Examination of parachute canopies after experimental tests have revealed the importance of parachute material mass and its distribution. Areas remote from overlapped seams have obtained higher temperatures than in the higher mass seam areas. The thermal heat sink of a given component is significant in determining the final temperature attained by that component.

When the decelerator is being heated, the maximum temperature the surface can attain is the equilibrium temperature—i.e. the temperature resulting from a balance between convective heating and radiation cooling. Therefore the maximum temperature which may develop is strongly dependent on the film heat-transfer coefficient and the emittance of the material. The radiation equilibrium temperature closely approaches the adiabatic wall temperature at low Mach numbers where the total temperature is small. The departure is significant above Mach number 2·0 due to the T^4 variation.

For the "actual" or "instantaneous" temperature, the convection heat transfer coefficient, the surface emittance, and the thermal diffusivity of the decelerator material must be known for each point of the trajectory. The present experiments were designed to provide information only about the convective heat-transfer coefficient.

Heat will be transferred from the hot gas to the screen. The heat transfer coefficient for a mesh configuration is expressed by the following dimensionless relationship:

$$Nu = f(Re, Pr, Ma_f, Po). \tag{1}$$

Since a sonic throat condition occurs for supercritical pressure ratios, it appears of advantage to use a sonic Reynolds number defined as

$$Re^* = \frac{\rho^* a^* d}{\mu^*} \tag{2}$$

where the viscosity μ^* is independent of the pressure p^* and a known function of the temperature T^*.

The Prandtl number Pr, whose value for air is approximately 0·7 under normal atmospheric conditions, deviates up to ± 10 per cent from this value to temperatures of approximately 6000°R. Thereafter the deviations become larger [4]. A temperature 6000°R corresponds to the stagnation conditions at $Ma_f = 10$ and 50000 ft altitude. At altitudes up to 400000 ft the stagnation temperatures for $Ma_f \leqslant 10$ will be below 6000°F. The small temperature differences employed yield the result that the deviations of the Prandtl number from the value 0·7 may be neglected in this paper.

The flight Mach number Ma_f has only an indirect influence upon the heat transfer to the canopy. In conjunction with the flight altitude, it fixes the stagnation pressure and temperature downstream of the shock. The Mach number appearing in the relation for the Nusselt number should be one indicating the flow conditions downstream from the wire grid because the upstream Mach number gives no information on downstream conditions for a supercritical pressure ratio. It is then more straightforward to use the pressure ratio P_{up}/P_{down} in place of a Mach number.

The porosity† Po is used as a parameter describing the geometry of the wire screen.

The purpose of the experiments described in this paper is to establish the relationship between the average convective Nusselt number, the Reynolds number Re_d^*, the pressure ratio P_{up}/P_{down}, and the porosity Po for a fluid with a Prandtl number equal to 0·7.

2. EXPERIMENTAL FACILITY

(A) *Low density wind tunnel*

Figure 2 shows the experimental facility used. A small subsonic wind tunnel was constructed to simulate the flow rates and reduced density

† Porosity is defined geometrically as the ratio of open area to total area of the forward-facing surface of the retardation device.

levels characteristic of the operation of supersonic parachutes. A small duct 2 in. dia., in which the flowmeter was located, was expanded into an 8 in. o.d. stilling chamber prior to the entrance of the test section. A mechanical vacuum pump-blower combination, with two interchangeable blowers, provided the necessary flow.

The open system is shown schematically in Fig. 3. The system draws air from the laboratory

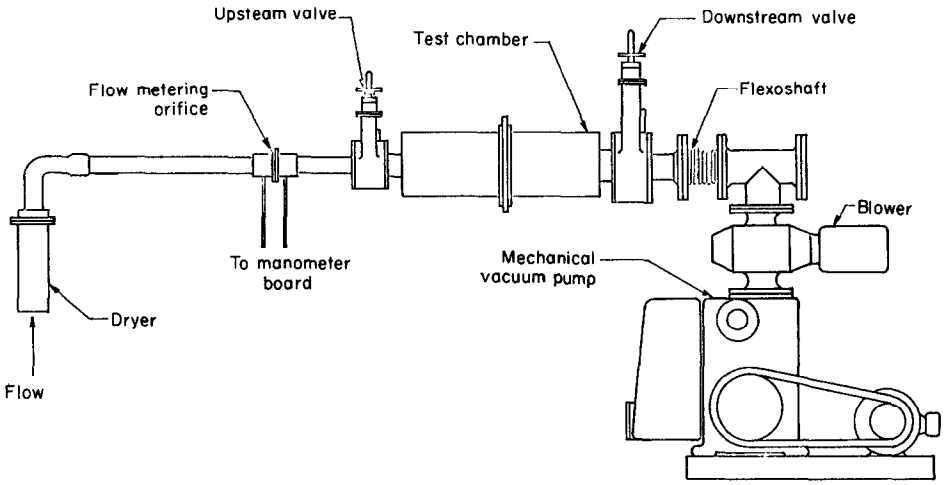

FIG. 3. Sketch of experimental facility.

room. It is composed of five components: air dryer, flow metering device, upstream and downstream valves, test chamber, and vacuum pump combination. The air dryer is an open-ended cylinder filled with calcium sulfide and one layer of glass wool. Two sharp-edged flat-plate orifices, one $\frac{1}{2}$ in. i.d., and the other $\frac{1}{8}$ in. i.d., were employed as flow metering devices for the range of Reynolds numbers anticipated. The mass flow through the system is found by measuring the pressure drop across each device when in use.

The corresponding ranges for each device are

$\frac{1}{8}$ in. orifice $\quad 1 < Re^* < 100$

$\frac{1}{2}$ in. orifice $\quad 80 < Re^* < 2000.$

The manometer board was constructed with three U-tubes. The first was filled with oil, giving the pressure drop between the entrance of the dryer and the flow metering device. The other two were filled with oil and mercury respectively to measure the pressure drop across the flow meter. The feed lines were fitted with valves to permit readings to be made with either oil or mercury. This allowed much larger ranges of Reynolds numbers to be covered with each device.

Two manually adjusted Temescal high-vacuum gate valves were installed in the system. The upstream valve was used to throttle the flow and provided the main adjustment for upstream pressure. The downstream valve could be used to change the pressure ratio.

The test chamber is shown in an exploded view in Fig. 4. In order to achieve uniform flow, a porous plate and fine mesh screen were encased in the upstream end. The central part of the porous plate was blanked off to further generate uniformity of flow. A mesh screen (60 wires per in.) was inserted 1·5 in. downstream to further break up the flow and reduce the scale of turbulence in the chamber.

The downstream half of the chamber was

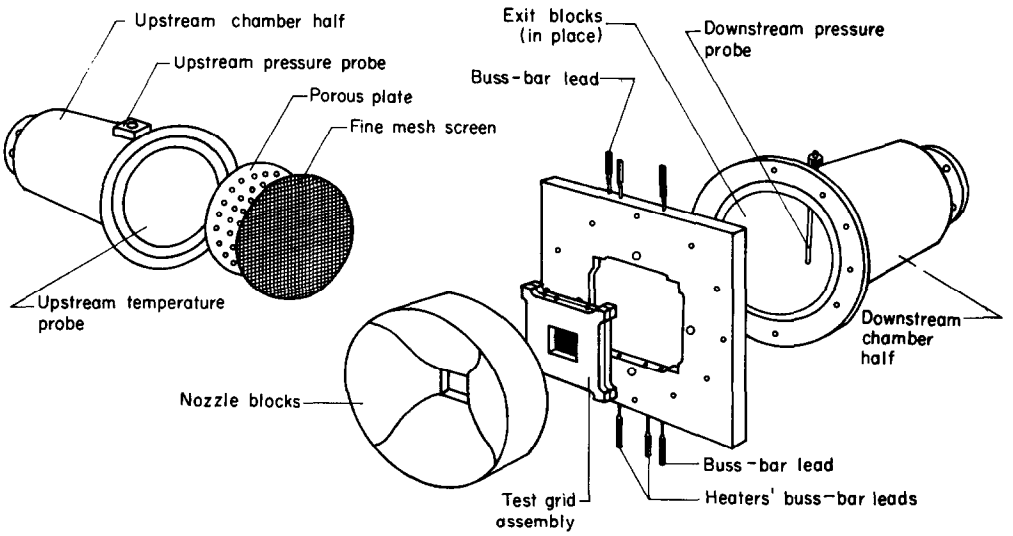

FIG. 4. Exploded view of test chamber.

fitted with wooden exit blocks to provide a straight expansion angle to 5° leading to the pump. This prevented an abrupt expansion just aft of the test grid and provided a closer approximation to parachute performance.

An aluminum plate with a square cavity in the middle was located between the two chamber halves. The test section was mounted in this cavity (Fig. 5). The nozzle block was immediately upstream of the aluminum plate and attached to it (Fig. 6) and was machined from a linen phenolic rod, sanded and hand-polished in order to keep the roughness as low as possible. The primary concern in designing the nozzle block was to minimize the boundary-layer thickness at the edge while preventing separation. The method of computing the nozzle profile was to compute the family of streamlines for the step geometry. To calculate the boundary-layer thickness and to get some idea if separation occurs, an integral solution to the boundary-layer equations was chosen. The method of Timman, given in [6], was used, as it allowed for the large pressure variations that appear in a nozzle. The optimum shape produced a minimum initial boundary layer thickness of

$$\delta\,(\text{in.}) = 0{\cdot}042/\sqrt{(Re_1)} \qquad Re_1 = \frac{\rho_1 u_1 d}{\mu_1}$$

at the nozzle block exit, with ρ_1, u_1 and μ_1 also evaluated at the nozzle block exit.

A total pressure probe was installed upstream of the test grid in the stilling chamber, and a static pressure probe was inserted into the wall of the exit block, flush with the wall. The upstream operating pressure and temperature determined the sonic Reynolds number, Re^*.

Two-vacuum-pump combinations were selected in order to study the influence of the pressure ratio on the heat transfer coefficient. The first was the Dresser RSS 120–150 matched blower and pump. Its intake operating range is from 10^{-2} mm of mercury to atmospheric pressure. The pump-blower combination maintains a constant pumping speed of 110 ft^3/min for inlet pressures down to $\frac{1}{2}$ mm of mercury, below which the pumping speed drops appreciably. This combination is the one which has been used mainly throughout these experiments.

The second vacuum-pump combination selected was the Dresser RS-260 DS-150 matched blower and pump. The pumping speed reaches a maximum of 240 ft^3/min at an inlet pressure of 0·5 mm of mercury and decreases to 170 ft^3/min at an inlet pressure of 100 mm of mercury; when the inlet pressure decreases below 0·1 mm of mercury, the pumping speed diminishes very fast to reach the value 0 at an inlet pressure of 2×10^{-3} mm of mercury. A Flexishaft coupling was installed just ahead of the pump (Fig. 3) to eliminate vibration in the wind tunnel.

(B) *Test section*

The test grid assembly is pictured in Fig. 5. The housing blocks inserted in the square cavity of the aluminum plate were modeled of Scotchcast Brand Resin No. 250, capable of withstanding temperatures of 250°F—well above operating temperatures. The contact surface between plastic and metal was kept small to minimize conduction loses. The flow cross-section was $\frac{3}{4} \times \frac{3}{4}$ in. The square configuration was chosen to eliminate the extreme difficulty of producing uniform heat generation in a circular geometry.

The stainless steel test screens were cut from woven wire screens and silver-soldered to the copper pieces shown in Fig. 7. The lateral sides of the wires were also silver-soldered to provide paths of uniform length and, with this, of the same electrical resistance; thus, uniform heating could be obtained. Also, no difference in the electrical potential should exist between two wires at any location where they touch.

Stainless steel was selected because of its relatively large resistivity, its high temperature resistance coefficient, and its strength, which allow smaller deformations under the influence of drag forces. The porosities were selected from those commercially available.

(C) *Instrumentation*

The instrumentation required for the test apparatus is of three types: temperature, pressure and electrical.

Three screens have been used, with the following properties as detailed in Table 1.

Table 1

	Screen 1	Screen 2	Screen 3
Diameter	0·0065 in	0·007 in	0·0055 in
Wires/in.	70	60	80
Geometric porosity	29·8%	33·9%	31·4%
Effective porosity†	0·329	0·336	0·325

Temperatures were sensed by 30 gauge iron–constantan thermocouples individually calibrated to an accuracy of $\pm 0{\cdot}1$°F. The calibration points were fitted with least square curves so that the temperature could be calculated on a computer. No significant error is initiated by this procedure.

The upstream total temperature was sensed by a probe positioned two inches upstream of the nozzle block and located in the geometric center of the stilling chamber.

The total upstream pressure was measured by an Alphatron Type 530 vacuum gauge made by NRC Equipment Corporation. This instrument utilizes an ionization chamber with a radium source. It has seven decade scales ranging from 1000 to 0·001 mm or mercury. The accuracy is 2 per cent of full scale reading.

All electrical measurements, including the thermocouple millivolt readings, were made with a Dymec 2010A digital acquisition system. This system measures analog data including a.c. and d.c. voltages. Accuracy is 0·01 per cent of full scale reading. The voltages measured were averaged over a period of one second.

† This is a different porosity used by Heinrich [7] for aerodynamic studies. The effective porosity C is defined as

$$C = \frac{U}{V}$$

with U the average velocity of the air through the screen and V a fictitious velocity, defined as

$$V = \sqrt{\left(\frac{2\Delta p}{\rho^2}\right)}$$

where Δp is the pressure drop across the screen ($P_{up} - P_{down}$) and ρ the density of the air downstream of the screen.

Current flow was found by employing precision shunts, each individually calibrated before use.

Owing to the inductive effects created by the woven mesh elements, d.c. power was used for all tests. The power was supplied by two six-volt storage batteries wired in parallel for the high Reynolds number and from a specially-wired six-volt battery, giving three parallel-connected, two-volt cells, for the low Reynolds number.

In order to shield the test screen from electrical noises a metal screen was mounted far downstream of the test mesh. This screen, in conjunction with the metal screen, used to increase the uniformity of the flow and the pipe system formed a closed, noise-isolated volume.

3. EXPERIMENTAL STUDIES

Heat-transfer measurements

The goal of this experiment was to find the relation between the average heat-transfer coefficient h and the sonic Reynolds number Re^*. The average heat-transfer coefficient is given by

$$h = \frac{Q/A}{t_w - t_{aw}} \tag{3}$$

where Q is the heat input, given by the ohmic heating I^2R, with I being the intensity of the electrical current and R the electrical resistance of the screen, and A the total area of the wires forming the test screen.

The governing equations are given by a heat balance at the screen,

$$I^2R = hA(t_w - t_{aw}) \tag{4}$$

and by the well-known relation

$$R = R_{aw}[1 + \alpha(t_w - t_{aw})]. \tag{5}$$

From the variables appearing in the equation, I and R are easily measured by using a calibrated shunt and a standard resistance. Further, with a previous calibration of the resistance R as a function of the temperature, α could be found and, knowing R and α, t_w and t_{aw} could be read from the calibration curve.

It can be shown that in the case that the reference value of the resistance R_{aw} does not change during a running period, the resistance R should be a linear function of the square of the current intensity, I^2. If one measures the electrical resistance R for different intensities and finds corresponding points to be on a straight line, then one can extrapolate this line to the value $I = 0$ and obtain a reference value R_{aw} for each run. In this case the heat-transfer coefficient h is given by

$$h = \frac{RR_{aw}\alpha \tan \beta}{A} \tag{6}$$

(β is the angle indicated in Fig. 8).

As a general rule R was measured during each run for five or six values of the current (see Fig. 8).

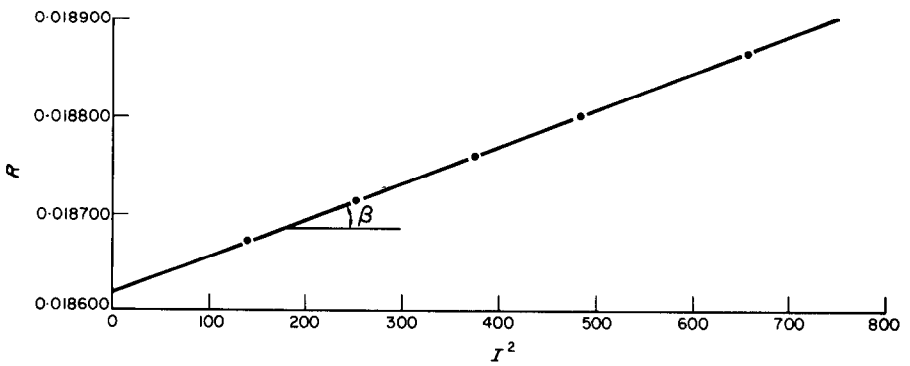

FIG. 8. Example of extrapolation technique used to obtain R_0.

The normal range of change of I was from 10 to 40 amp for the higher Re^* numbers and between 4 and 10 amp for the small Re^*. For the practical calculations the straight line was fitted, using the criterion of the least square, with the aid of the computer.

The sonic Reynolds number Re^* was changed by varying the upstream pressure. When the pump–blower combination RSS-120-150 was used, the pressure ratio P_{up}/P_{down} could be maintained almost constant for all three screens —independent of the upstream pressure P_{up}— as shown in Fig. 9. The small oscillations shown may be due to small changes in the efficiency of the pump–compressor system with the input pressure and to the small errors in readings of the upstream and downstream pressures.

4. DISCUSSION OF RESULTS

The dimensionless Nusselt number,

$$Nu = \frac{hd}{k}, \tag{7}$$

based on the wire diameter, has been used instead of the dimension-dependent heat-transfer coefficient. The results experimentally obtained are shown in Fig. 10, where the Nusselt number Nu has been plotted as a function of the sonic Reynolds number Re^*. Although the influence of the pressure ratio P_{up}/P_{down} appears to be small, a tendency towards decreasing the dimensionless heat-transfer coefficient with increasing pressure ratio can be observed. This phenomenon seems to be logical since a decrease of the pressure ratio, while holding the upstream pressure constant, indicates a lower downstream static pressure which should affect the local heat-transfer coefficient in the manner noted.

No effects of the porosity Po on the average Nusselt number—within the relatively narrow range of porosities investigated—can be observed in Fig. 10.

It is of interest to compare the measured Nusselt numbers for a screen with Nusselt numbers obtained for flow across a cylinder. Figure 11 is the result of such a comparison.

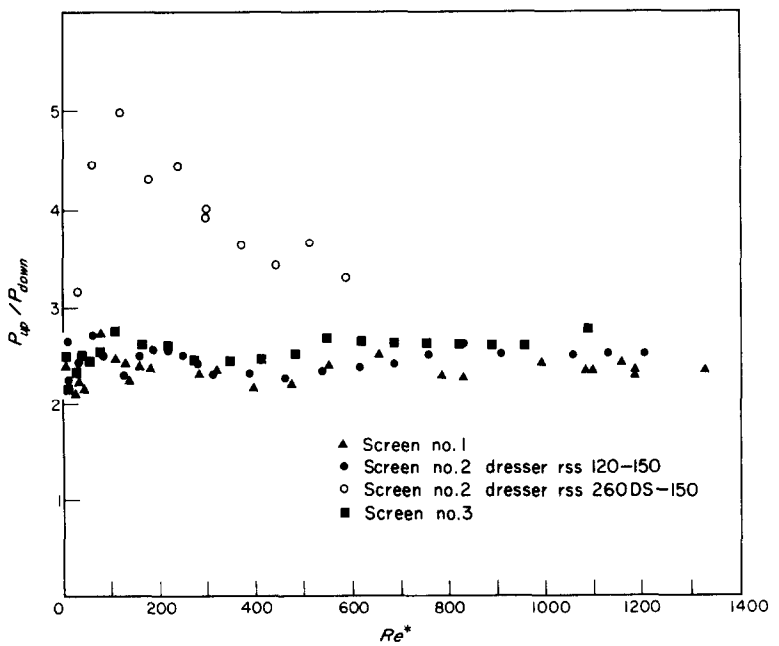

FIG. 9. P_{up}/P_{down} vs. Re^*.

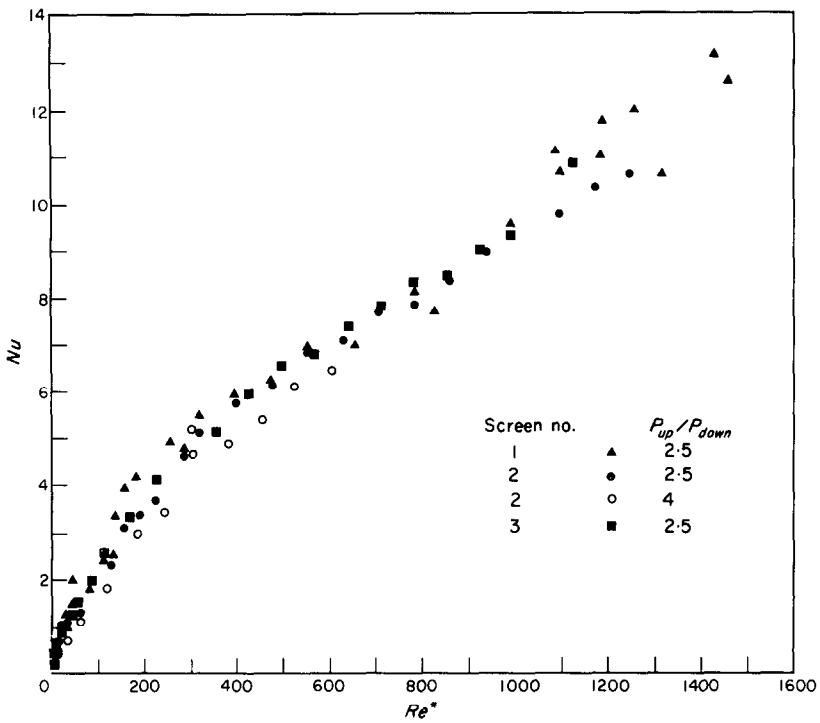

FIG. 10. Nusselt number vs. Re^*.

The lines in the figure represent average Nusselt numbers as a function of upstream Reynolds number, with the upstream Mach number as a parameter. These Nusselt numbers have been taken from [8]. The symbols in the figure refer to the present experimental measurements. For this purpose the Reynolds number Re_1, based on flow conditions at the nozzle block exit and on the wire diameter, has been obtained from the sonic Reynolds number Re^*. The Mach number Ma_1 was also calculated at this location. The Knudsen number† calculated from the relation

$$Kn = \frac{Ma_1}{Re_1} \tag{8}$$

is also indicated in Fig. 11 as abscissa.

One should be careful in drawing conclusions from a quantitative comparison of the curves with the lines in this figure because of the difference in flow condition on a single cylinder and on a screen. For the same upstream flow condition, for instance, the maximum velocity outside the boundary layer on the cylinder is larger for the screen than for the single cylinder. Nevertheless a qualitative comparison certainly can be made and the figure indicates that rarefaction effects become important for Reynolds numbers lower than a value of order 100. This rarefaction effect also explains why the Nusselt numbers continuously decrease at about the same rate with decreasing Reynolds number, whereas in incompressible flow ($Ma = 0$) the decrease of the Nusselt number diminishes as the Reynolds number approaches the value 1. The figure shows that the agreement between Nusselt numbers measured on the screens with values for a single cylinder is surprisingly good. At the highest Reynolds numbers investi-

† For plotting purposes in Fig. 11, the Mach number Ma_1 has been considered constant and equal to 0·185.

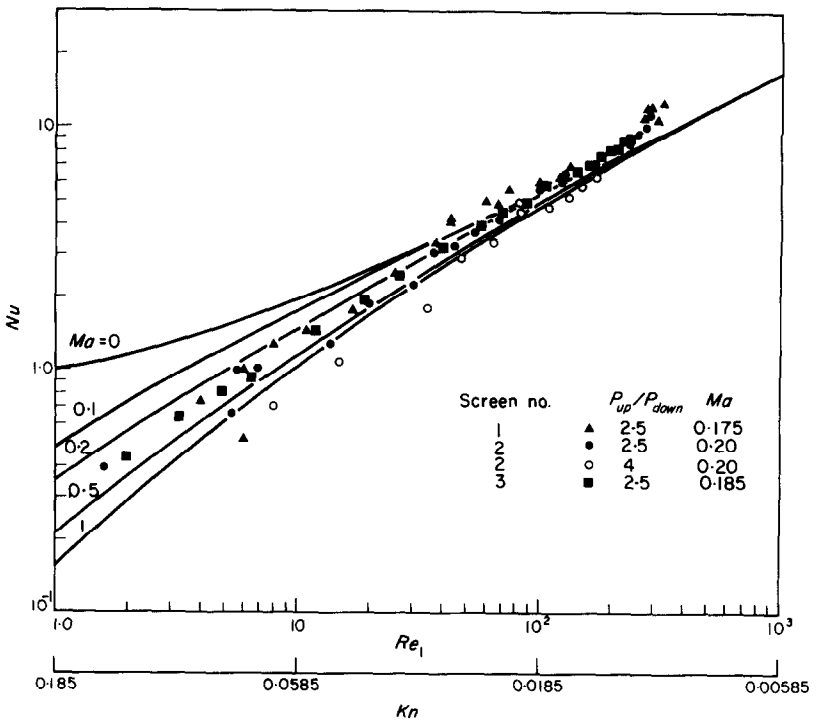

FIG. 11. Comparison of present results with results for a cylinder.

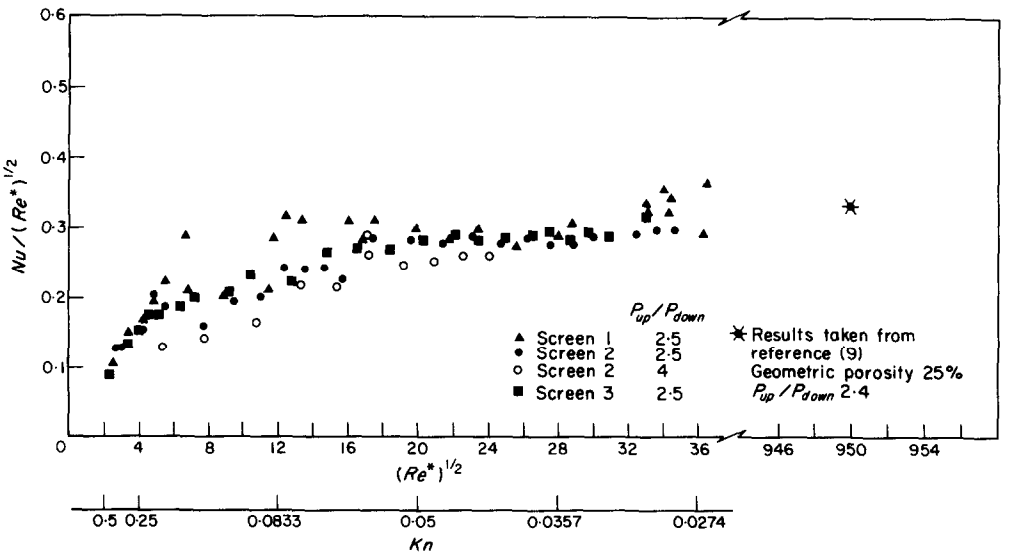

FIG. 12. $Nu/(Re^*)^{\frac{1}{2}}$ vs. $Re^{*\frac{1}{2}}$.

gated (beyond a value $Re_1 = 250$) a sudden increase in Nusselt number is indicated which is not evident on the curves for the single cylinder.

In Fig. 12 the ratio $Nu/(Re^*)^{\frac{1}{2}}$ has been plotted versus $(Re^*)^{\frac{1}{2}}$. Here the value $Nu/(Re^*)^{\frac{1}{2}}$ seems to be constant for Re^* larger than 400. Also included in this figure are the integrated results reported in [9]. In that study the local measurements were made on an enlarged woven mesh in which the individual fibers were 1 in. dia. The porosity and pressure ratio of the data in [9] closely match the present studies, while the sonic Reynolds number was considerably higher. The agreement between the integrated local values is very good.

Scott [10] derived the following expression describing the Nusselt number at the stagnation point of the wires in a screen from a laminar stagnation point boundary-layer analysis:

$$\frac{Nu^*\left(\frac{L+d}{L}\right)}{(Re^*)^{\frac{1}{2}}} = 2 \times 0{\cdot}496. \qquad (9)$$

Here L is the distance between the centers of two consecutive parallel wires in the screen. In Fig. 13 this relation is compared with the measurements on the three screens. For sonic Reynolds numbers Re^* above a value of 400, the average Nusselt number is one half the value given in equation (9). It is to be expected [9] that the average value of the Nusselt number is less than the maximum value found at the stagnation point. The factor $\frac{1}{2}$ is also found on single cylinders [11]. It is recommended that the equation

$$\frac{Nu^*\left(\frac{L+d}{L}\right)}{(Re^*)^{\frac{1}{2}}} = 0{\cdot}5 \qquad (10)$$

be suggested for the calculation of average Nusselt numbers of screens with the porosity range exceeding that in our experiments. For sonic Reynolds numbers below 400, the average Nusselt numbers drop off with decreasing Reynolds number as a consequence of the rarefaction effects.

Figure 13 also contains the integrated local

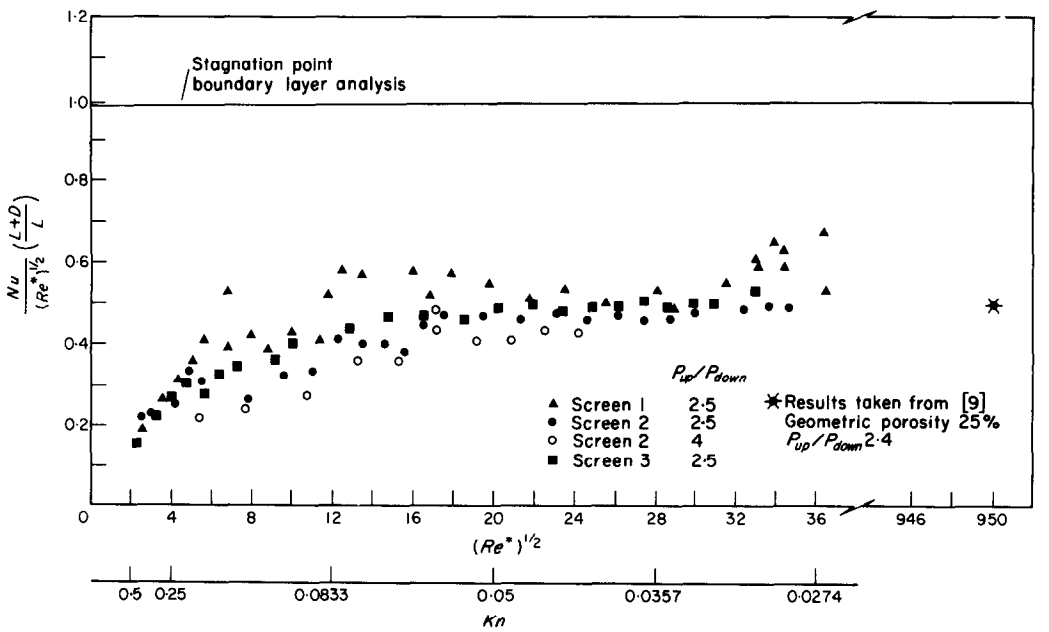

FIG. 13. Comparison of experimental results with theoretical prediction.

heat-transfer coefficients of [9]. The agreement of integrated local values with the present average values is quite heartening.

5. CONCLUSIONS

Convective heat-transfer experiments have been performed on three woven wire mesh screens simulating porous parachute cloth with porosities of 29·8, 31·4 and 33·9 per cent. Average Nusselt numbers were measured as a function of sonic Reynolds number at a ratio of 2·5 of the upstream total to the downstream static pressure. The results are presented in Figs. 10 through 13. They indicate the Nusselt number to be proportional to $R_e^{*\frac{1}{2}}$, for Re^* larger than 400. Below this value of Re^* rarefaction effects begin to influence heat transfer. No effect of porosity on the average heat-transfer coefficient could be established within the range of porosities which were investigated and the accuracy obtained. The effect of varying the ratio of the upstream total pressure to the downstream static pressure was checked on one of the screens and was found to be small for values between 2·5 and 4. The Nusselt numbers for screens are shown to exhibit a behavior quite similar to the Nusselt number for a single cylinder in cross flow. The relation

$$\frac{Nu^* \quad \dfrac{L+d}{L}}{(Re^*)^{\frac{1}{2}}} = 0{\cdot}5$$

appears to be an acceptable representation of the average Nusselt numbers on screens for sonic Reynolds number above 400 for which rarefaction effects are not present.

ACKNOWLEDGEMENT

This paper presents the results of one phase of research supported by the Air Force Flight Dynamics Laboratory, Wright-Patterson AFB, Ohio under Contract F33615-67-C-1028.

REFERENCES

1. DE. HRITZAY and R. WIANT, Wire cloth structure for a radiating re-entry vehicle, AVCO-Everett Research Report 123.(1962).
2. A. C. KYSER, The Rotornet: a high-performance hypersonic deceleration for planetary entry, NAS CR-247, June (1965).
3. J. C. Y. KOH and J. P. HARTNETT, Measured pressure distribution and local heat transfer rates for flow over concave hemispheres, presented at the Semi-Annual Meeting of the American Rocket Society, Los Angeles, California, 9–12 May (1960).
4. C. F. HANSEN, Approximations for the thermodynamic and transport properties of high-temperature air, NACA Technical Note 4150.
5. S. T. MCCOMAS, Heat transfer and pressure drop in Laminar flow through a circular tube under continuum and rarefied conditions, Ph.D. Thesis, University of Minnesota (1964).
6. L. ROSENHEAD, *Laminar Boundary Layers*, Oxford University of Minnesota (1966).
7. H. G. HEINRICH, The effective porosity of parachute cloth, Technical Report AFFDL-TR-65-102, University of Minnesota (1966).
8. L. V. BALDWIN, V. A. SANDBORN and J. C. LAURANCE, Heat transfer from transverse and yawed cylinders in continuum, slip and free molecule air flows, *J. Heat Transfer*, May (1960).
9. C. J. SCOTT and M. RUIZ-URBIETA, Experiments on the distributions of local pressure and heat transfer on a grid simulating a parachute fabric, *J. Aircraft*, **5** (1968).
10. C. J. SCOTT, The prediction of material temperatures on woven retardation devices, AFFDL-TR-67-170 or University of Minnesota HTL-TR-71(1967).
11. E. R. G. ECKERT and J. M. DRAKE, JR., *Heat and Mass Transfer*, McGraw-Hill, New York (1959).

Résumé—Des études expérimentales de transport de chaleur ont été effectuées sur trois toiles simulant un parachute poreux. Le nombre de Nusselt moyen a été mesuré en fonction du nombre de Reynolds sonique. La gamme du nombre de Reynolds sonique s'étendait de 5 à environ 1400. Trois porosités différentes et deux rapports de pression différents ont été utilisés.

La relation

$$\frac{Nu^*}{(Re^*)^{\frac{1}{2}}} \quad \frac{L+D}{L} = 0{,}5$$

paraît être une représentation acceptable du nombre de Nusselt moyen sur la toile pour un nombre de Reynolds sonique supérieur à 400. En dessous de ce nombre de Reynolds sonique, les effets de raréfaction influencent le nombre de Nusselt moyen. Aucun effet de la porosité ne pouvait être détecté, tandis que l'influence du rapport de la pression amont à la pression statique aval était faible pour les deux valeurs essayées.

Zusammenfassung—Experimentelle Wärmeübergangsuntersuchungen wurden an drei Gittern durchgeführt in Nachbildung eines porösen Fallschirms. Die mittlere Nusseltzahl wurde als Funktion der sonischen Reynolds–Zahl gemessen. Der Bereich der sonischen Reynolds–Zahl erstreckte sich von 5 bis etwa 1400. Drei verschiedene Porositäten und zwei verschiedene Druckverhältnisse wurden benützt.

Die Beziehung

$$\frac{Nu^*}{(Re^*)^{\frac{1}{2}}} \frac{L+D}{L} = 0{,}5$$

scheint eine annehmbare Wiedergabe der mittleren Nusselt–Zahl am Gitter für sonische Reynolds–Zahlen über 400 darzustellen. Unterhalb dieser sonischen Reynolds–Zahl beeinflussen Verdünnungseffekte die mittlere Nusselt–Zahl. Kein Einfluss der Porosität konnte gefunden werden, während der Einfluss des Verhältnisses des Druckes stromaufwärts zum statischen Druck stromabwärts in den beiden untersuchten Fällen klein war.

Аннотация—Проведено экспериментальное исследование теплообмена на трех модельных экранах, имитирующих пористый парашют. Среднее число Нуссельта измеряется как функция звукового числа Рейнольдса. Диапазон звукового числа Рейнольдса расширен от 5 до почти 1400. В работе использовались три различных значения пористости и два различных отношения давлений.

Соотношение $[Nu/(Re)^{\frac{1}{2}}][(\mathscr{L} + D)/\mathscr{L}] = 0{,}5$ представляется приемленым для выражения среднего числа Нуссельта на экране при звуковом числе Рейнольдса свыше 400. Ниже этого значения звукового числа Рейнольдса разрежение начинает влиять на среднее число Нуссельта. Влияния пористости не обнаружено, а влияние отношения статистического давления в верхнем течении к статистическому давлению в нижнем течении для двух исследованных величин не обнаружено.